Supplementary Materials

1 Manufactured SIPs

A number of stable SIPs were manufactured using various PDMSs, stabilising agents, and solvents. These are summarised in Table S1 below. Several emulsions were labelled as 'low viscosity' - while the viscosity was not measured, these emulsions flowed freely with a viscosity comparable to glycerol. The emulsions containing KE-103 was used for manufacturing particles.

SIP	PDMS	Aqueous Solvent	Solvent wt%	Stabilising Agent(wt% in Emulsion)	Crosslinking	Comments
SIP1	Semicosil 949 UV	Water	50%	9011 (1%)	UV Light	
SIP2	Semicosil 949 UV	3wt% K_2CO_3	50%	9011 (1%)	UV Light	Optionally add 0.25g/L of thymol blue to the aqueous phase to visualise CO_2 uptake.
SIP3	Semicosil 949 UV	30wt% K_2CO_3	50%	9011 (1%)	UV Light	
SIP4	Semicosil 949 UV	30wt% K_2CO_3	40%	Ethanol (2.5%)	UV Light	Small particle size and low viscosity emulsion.
SIP5	KE-106	30wt% K_2CO_3	50%	9011 (1%)	Heat	
SIP6	KE-106	30wt% K_2CO_3	50%	Ethanol (2.5%)	Heat	
SIP7	Sylgard 184	30wt% K_2CO_3	50%	Ethanol (2.5%)	Heat	
SIP8	KE-103	3wt% K_2CO_3	25%	Ethanol (1.25%)	Heat	Optionally add 0.25g/L of thymol blue to the aqueous phase to visualise CO_2 uptake. Low viscosity emulsion.
SIP9	KE-103	30wt% K_2CO_3	25%	Ethanol (1.25%)	Heat	Low viscosity emulsion.
SIP10	Semicosil 949 UV	10wt% K_2CO_3	50%	9011 (1%)	UV Light	
SIP11	50wt% SMS-042, 50wt% DMS-V31 0.1wt% DMPA Crosslinker	DMEDAH Formate	50%	5225C (1%)	UV Light	Solid DMPA was dissolved in SMS-042 using a sonicator before polymers were mixed.

Table S1: Summary of Manufactured solvent impregnated polymers.

1.1 Internal Particle Size Distribution

The internal droplet size inside SIPs varied substantially depending on the PDMS, stabilising agent and solvent used. In Figure S1 below, the microscopic structure of 2 stable SIPs with particle size ranging from 1 µm to several 100 µm are compared; the SIP shown in Figure 2 of the paper is also reproduced. The left-hand column shows images of the precursor emulsions, while the right-hand column shows images of the crosslinked emulsions. The internal particle size distribution for each of these materials was estimated using ImageJ, and is shown in Figure S2.

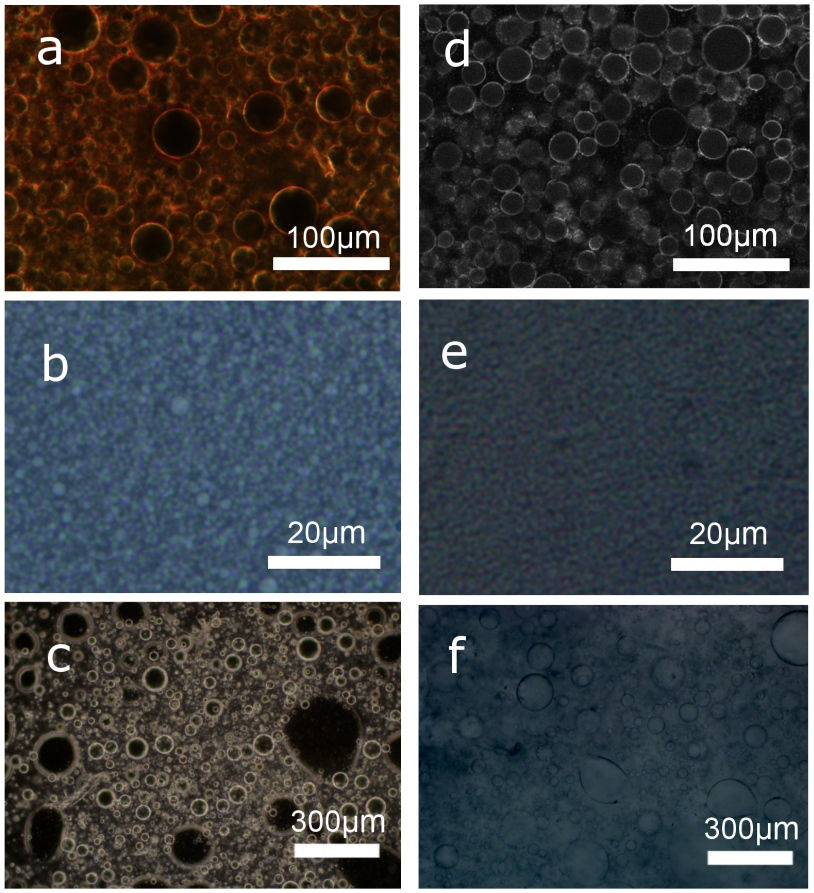

Figure S1: (a)-(c) are microscopic images of precursor emulsions for SIP10, SIP4 and SIP8 in Table S1 respectively. (d)-(f) are images of crosslinked SIP gels for SIP10, SIP4 and SIP8 respectively.

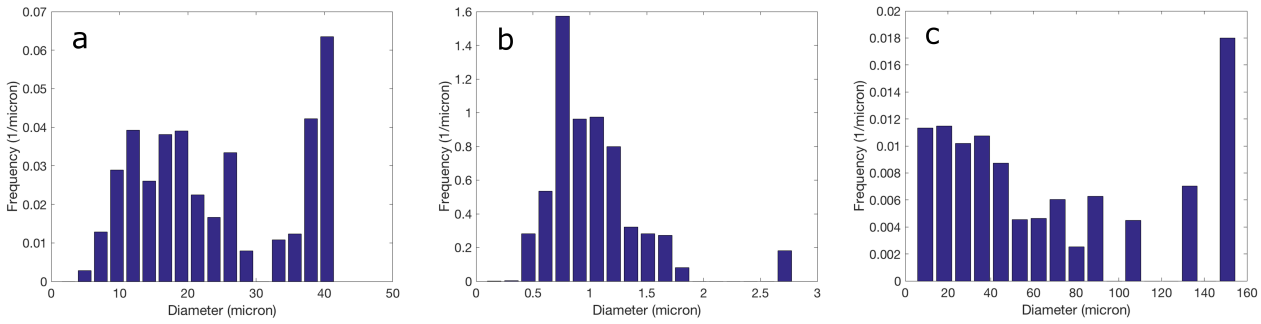

Figure S2: Volume averaged particle size distributions for (a) SIP10, (b) SIP4 and (c) SIP8 from Table S1, calculated via image analysis on photographs of emulsions using ImageJ.

1.2 SIP Particles

Figure S3 shows typical SIP particles, manufactured according to the methods discussed in the Experimental section of the paper. Figure S4 shows the particle size distribution for a batch of particles, calculated by estimating the diameter of several 1000 particles using ImageJ.

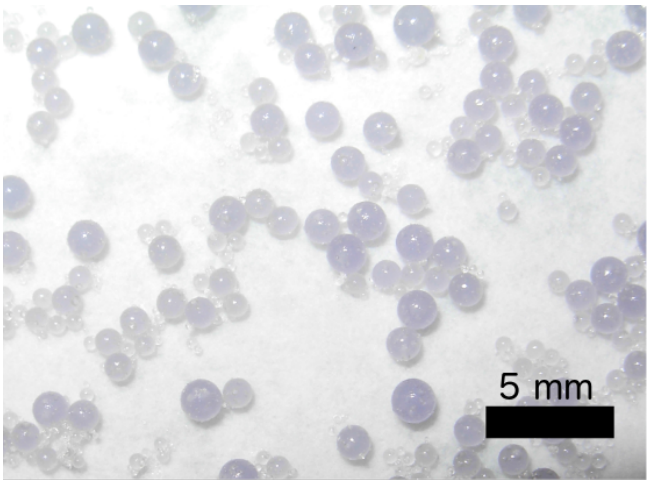

Figure S3: SIP particles composed of SIP8 in Table S1.

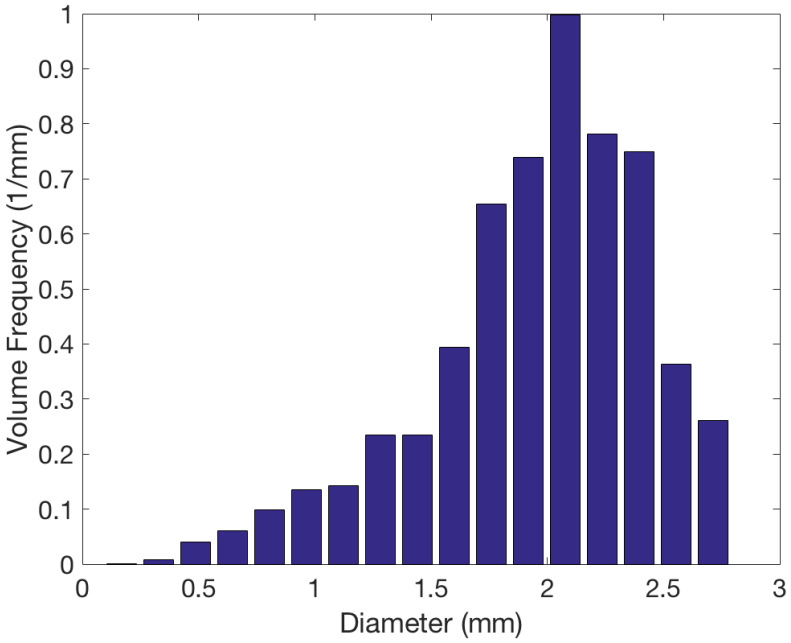

Figure S4: Volume-weighted particle size distribution of particles composed of SIP8.

.

Model Development

2 Model Derivation

2.1 Assumptions

- We ignore changes in density, temperature, gas solubility and diffusivity that may occur during the absorption process.
- The diameter of solvent droplets are much less than the length scale over which macroscopic changes occur, so a continuum model is justified.
- The solvent reacts with the gas via a second order reaction - first order in both the active species and in the absorbed gas.
- Interfacial mass transfer resistance at the polymer-liquid surface is ignored. Thus the concentrations of gas at the interface are related by:

$$\frac{c_s}{\mathcal{S}_s} = \frac{c_l}{\mathcal{S}_l} \tag{1}$$

- The solvent is perfectly trapped inside the polymer matrix, and so no solvent escapes the material or diffuses within it.
- Diffusional resistance inside the immobilised droplets is accounted for via an effectiveness factor,

$$\xi = \frac{\phi' \coth \phi' - 1}{\phi'^2/3} \tag{2}$$

  where $\phi' = r_{\text{drop}}\sqrt{k_2 w/\mathcal{D}_l}$ is the local Thiele modulus.[1] The rate of reaction inside a droplet is equal to the rate of reaction if the concentration profile were constant in space, multiplied by the effectiveness factor. Because diffusional resistance inside the droplets is considered significant, the concentration of gas inside the droplets is not constant in space, and inside each droplet it is less than the concentration at the surface of the droplet, c_l.
- Diffusional resistance inside the polymer is ignored, and so the concentration inside the polymer is considered constant on a local scale, and is equal to c_s. This is reasonable, as the permeability in the polymer is typically much greater than the permeability in the liquid. Furthermore, local diffusional resistance in the polymer is only significant when the reaction is fast, and under these conditions the model will collapse to a moving front model which is not controlled by the local diffusional or reaction resistance (see Ho et al.[2]).

2.2 Mass Balance

Consider the thin linear slice of SIP shown in Figure S5. Assume it has unit cross-sectional area. Then the rate of change of *physical* or *free* gas molecules (e.g. unreacted CO_2 molecules) in this slice is:

$$\Delta x \varepsilon \frac{\partial c_s}{\partial t} + \Delta x \xi (1-\varepsilon)\frac{\partial c_l}{\partial t}. \tag{3}$$

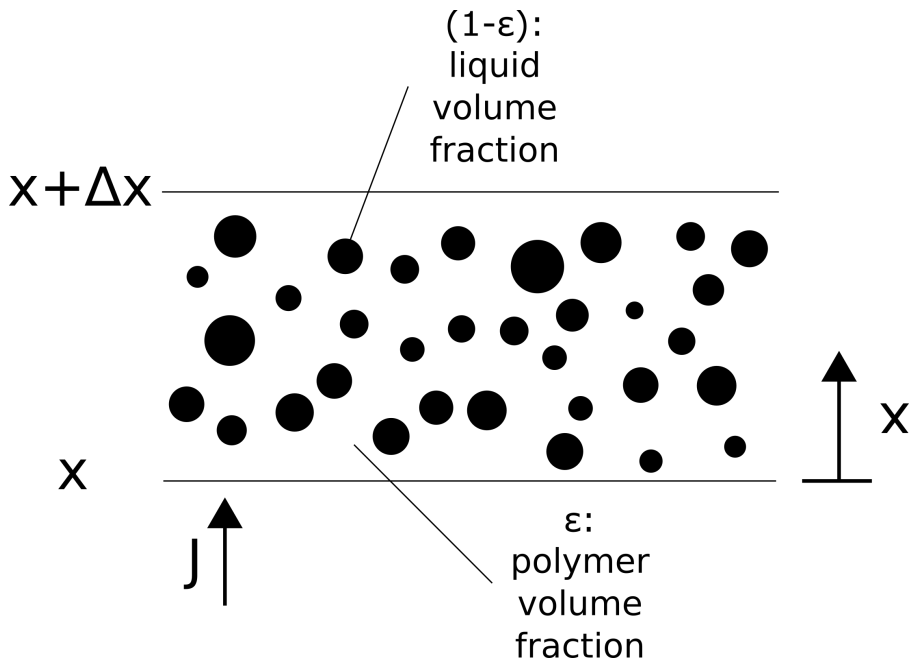

Figure S5: A thin slice of SIP, indicating coordinate choice, volume fraction definition, and direction of gas flux.

where ξ is given by Eq. (2) - this appears in Eq. (3) because the average concentration of free gas molecules inside a droplet is reduced by a factor of ξ when there is local diffusional resistance. This may be simplified to:

$$\left(\varepsilon\frac{\mathcal{S}_s}{\mathcal{S}_l}+\xi(1-\varepsilon)\right)\frac{\partial c_l}{\partial t}\Delta x \tag{4}$$

The net diffusive flow of free gas molecules into this slice is:

$$\mathcal{D}_s\varepsilon\left(-\frac{\partial c_s}{\partial x}\bigg|_x-\left(-\frac{\partial c_s}{\partial x}\bigg|_{x+\Delta x}\right)\right)+\mathcal{D}_l(1-\varepsilon)\left(-\frac{\partial c_l}{\partial x}\bigg|_x-\left(-\frac{\partial c_l}{\partial x}\bigg|_{x+\Delta x}\right)\right) \tag{5}$$

which may also be simplified to:

$$\left(\mathcal{D}_s\varepsilon\frac{\mathcal{S}_s}{\mathcal{S}_l}+\mathcal{D}_l(1-\varepsilon)\right)\left(-\frac{\partial c_l}{\partial x}\bigg|_x-\left(-\frac{\partial c_l}{\partial x}\bigg|_{x+\Delta x}\right)\right). \tag{6}$$

This expression

The net rate of reaction of free gas molecules inside the slice is:

$$-k_2\xi w c_l(1-\varepsilon)\Delta x \tag{7}$$

where w is the concentration of the reactive species inside the liquid which reacts with the free gas. This is typically a space- and time-dependent variable, and we will discuss it's dynamics later; for now note that the active species not diffuse, and also that the relation between the rate of gas reaction and the depletion of reactive species can be complex, especially if other reactions, such as buffers, occur simultaneously. Because the droplets are microscopic, w will be assumed to be constant inside each droplet (this is equivalent to a pseudo-first order assumption inside each droplet).

Combining all these terms, and dropping the subscript of c_l, the mass balance gives:

$$\left(\varepsilon\frac{\mathcal{S}_s}{\mathcal{S}_l}+\xi(1-\varepsilon)\right)\frac{\partial c}{\partial t}\Delta x = \left(\mathcal{D}_s\varepsilon\frac{\mathcal{S}_s}{\mathcal{S}_l}+\mathcal{D}_l(1-\varepsilon)\right)\left(\left.\frac{\partial c}{\partial x}\right|_{x+\Delta x}-\left.\frac{\partial c}{\partial x}\right|_{x}\right)-k_2\xi wc(1-\varepsilon)\Delta x \quad (8)$$

Divide by Δx and take $\Delta x \to 0$, and we get

$$\left(\varepsilon\frac{\mathcal{S}_s}{\mathcal{S}_l}+\xi(1-\varepsilon)\right)\frac{\partial c}{\partial t}=\left(\mathcal{D}_s\varepsilon\frac{\mathcal{S}_s}{\mathcal{S}_l}+\mathcal{D}_l(1-\varepsilon)\right)\nabla^2 c-k_2\xi wc(1-\varepsilon) \quad (9)$$

Or, to clear up the mess,

$$\frac{\partial c}{\partial t}=\mathcal{D}^{\text{eff}}\nabla^2 c-\xi k_2^{\text{eff}}wc \quad (10)$$

where

$$\mathcal{D}^{\text{eff}}=\frac{\mathcal{D}_s\varepsilon\frac{\mathcal{S}_s}{\mathcal{S}_l}+\mathcal{D}_l(1-\varepsilon)}{\varepsilon\frac{\mathcal{S}_s}{\mathcal{S}_l}+\xi(1-\varepsilon)} \quad (11)$$

and

$$k_2^{\text{eff}}=\frac{k_2(1-\varepsilon)}{\varepsilon\frac{\mathcal{S}_s}{\mathcal{S}_l}+\xi(1-\varepsilon)} \quad (12)$$

Now w is the concentration of reactive species, and (as this has no spatial mobility within the material) it may be modelled by:

$$\frac{\partial w}{\partial t}=f(c,w,\xi). \quad (13)$$

Note that w also changes in *space*, so ∂ is appropriate. An appropriate $f(\cdot)$ for the reaction of CO_2 with OH^- in a K_2CO_3-$KHCO_3$ buffer solution is derived below.

3 Numerical Solution

These equations were solved via a method of lines (MOL) approach using the DifferentialEquations.jl suite in Julia. The implementation was based on the excellent monograph of Hundsdorfer and Verwer[3].

- To model absorption into a flat SIP inside a petri dish, we modelled the SIP surface via a Dirichlet condition, and the bottom of the material via a Neumann condition.
- A second order spatial discretisation was used: these are commonplace for diffusion problems, and indeed almost identical systems have been modelled via exactly this approach before (c.f. Hundsdorfer and Verwer[3], particularly p. 64 and p. 206).
- The stiff `CVODE_BDF()` solver inside DifferentialEquations.jl, which interfaces with the popular backwards differentiation formulas in the CVODE solver.[4] This was necessary, as MOL discretisations of diffusion problems are often stiff (c.f. Hundsdorfer and Verwer[3], p. 64). An alternative stiff solver, `Rodas4()`, which uses a 4th order stably-stiff Rosenbrock method, was used in the dimensionless analysis below. Though it was substantially slower, as a pure-Julia implementation it proved more stable when implementing a continuous callback.

The PDE's were discretised on a vertex-centred grid with points labelled $j = 1 \cdots m+1$. The Neumann condition held at the boundary at point 1, while the Dirichlet condition held at the boundary at point $m+1$. The point spacing was $h = L/m$ (where L was the material thickness). For $j = 2 \ldots m-1$:

$$\dot{c}_j(t) = \frac{\mathcal{D}^{\text{eff}}}{h^2}(c_{j-1} - 2c_j + c_{j+1}) - k_2^{\text{eff}} c_j w_j \tag{14}$$

For the Neumann condition, we consider a ghost point at point $j = 0$ with concentration equal to c_2:

$$\dot{c}_1(t) = \frac{\mathcal{D}^{\text{eff}}}{h^2}(2c_2 - 2c_1) - k_2^{\text{eff}} c_1 w_1 \tag{15}$$

For the Dirichlet condition, note that $c_{m+1} = \mathcal{S}_l p$, where p is the gas partial pressure, so

$$\dot{c}_m = \frac{\mathcal{D}^{\text{eff}}}{h^2}(c_{m-1} - 2c_m + \mathcal{S}_l p) - k_2^{\text{eff}} c_m w_m \tag{16}$$

And of course, for all $j = 1 \ldots m$,

$$\dot{w}_j = f(c_j, w_j). \tag{17}$$

We can approximate the gas flux into the material using a second-order one-sided finite difference approximation:

$$J_{\text{surface}} = \left(\frac{\frac{3}{2}\mathcal{S}_l p - 2c_m + \frac{1}{2}c_{m-1}}{h}\right)\left(\mathcal{D}_s \varepsilon \frac{\mathcal{S}_s}{\mathcal{S}_l} + \mathcal{D}_l(1-\varepsilon)\right) \tag{18}$$

Integrating J_{surface} from time $t = 0$ with no gas in the material to saturation (with all physical properties set to 1 and $f = -cw$), the relative error in total gas absorption (compared to that predicted by the changes in concentration inside the material) is less than 10^{-3} for $m = 100$. In general m was chosen so that halving the grid-size had negligible effect on the solution.

4 Dimensional Analysis

As discussed in the paper, the SIP motif represents a tradeoff between improved gas flux increasing mass transfer, and decreased gas flux due to the presence of a saturated-zone building from the material surface (in the limit in which diffusional resistance through the saturated-zone dominates, the model collapses to the moving front model considered by Ho et al.[2]). To quantify these effects, the above model was put into dimensionless form, and was compared with a similar, dimensionless model for absorption into a static liquid. For a fair comparison, we compare a thin SIP layer with a liquid with identical surface area, and with volume chosen such that the total gas capacity of each are the same. We then calculate the time, t_γ, to reach some arbitrary degree of saturation γ (with $0 \leq \gamma \leq 1$), and we find the properties of each system that determine the ratio of these absorption times. We then apply these predictions to several hypothetical SIP materials. In what follows, we consider the simplest SIP chemistry: the gas reacts with 1-1 stoichiometry in a 2nd order reaction with the active species, w. The initial concentration of active species is w_0, and it is depleted over time as the reaction continues (i.e. it is not replaced by a buffer reaction.) We wil show below that the dimensionless analysis is also valid for a simple system in which the actives species is continually resupplied by other reactions.

4.1 Material Geometry

If the static liquid has thickness L, then a SIP material with the same gas capacity will have height:

$$L_{\text{SIP}} = L\left((1-\varepsilon) + \varepsilon \frac{c^*/w_0}{c^*/w_0 + 1}\frac{\mathcal{S}_s}{\mathcal{S}_l}\right)^{-1} \tag{19}$$

4.2 Transport Equations

In general, absorption into a SIP can be modelled via:

$$\frac{\partial c}{\partial t} = \mathcal{D}^{\text{eff}} \nabla^2 c - k_2^{\text{eff}} \xi w c \tag{20}$$

$$\frac{\partial w}{\partial t} = f(c, w, \xi). \tag{21}$$

For this analysis we consider the simplest scenario, in which we start with a fixed quantity of reactive species, which is consumed as it reacts with the gas with $1:1$ stoichiometry. Then

$$\frac{\partial w}{\partial t} = -k_2 \xi w c \tag{22}$$

Assuming we start with no gas absorbed, the initial and boundary conditions are:

$$c|_{t=0} = 0; \quad w|_{t=0} = w_0; \quad c_x|_{x=0} = 0; \quad c|_{x=L_{\text{SIP}}} = c^*. \tag{23}$$

The pde's describing absorption of gas into a static fluid are similar; for the absorbing gas, we have:

$$\frac{\partial c}{\partial t} = \mathcal{D}_l \frac{\partial^2 c}{\partial x^2} - k_2 c w. \tag{24}$$

We make the same assumptions about the solvent chemistry as before: the only difference is that in this case the reactive species is free to diffuse inside the liquid. In many systems of industrial interest we can make a *pseudo-first order* assumption: we suppose w changes slowly enough for spatial inhomogenieties in w to be smoothed out. For the second-order system under consideration, this will occur whenever $w_0 \gg c^*$, in other words when chemical solubility is much greater than physical solubility: a very common situation. (More rigorously, in an infinitely deep liquid the pseudo-first order assumption is valid whenever $\sqrt{\pi k_2 t w_0/4} \ll w_0/c^*$.[5] Because of the different scaling of w_0 on either side of the inequality, this is equivalent to $w_0 \gg c^*$ provided the material is not too thick.) Under this regime, w only depends on time, and varies according to:

$$\frac{dw}{dt} = -k_2 w \frac{1}{L} \int_0^L c(x) dx. \tag{25}$$

The boundary and initial conditions are

$$c|_{t=0} = 0; \quad c_x|_{x=0} = 0; \quad c|_{x=L} = c^*; \quad w|_{t=0} = w_0. \tag{26}$$

4.3 Dimensionless Form of Transport Equations

We now transform each equation into a dimensionless form. The dimensionless variables for the static liquid are defined as follows:

$$c = c^* \bar{c}; \quad w = w_0 \bar{w}; \quad t = (k_2 c^*)^{-1} \bar{t}; \quad x = L\bar{x}. \tag{27}$$

With these definitions, equations (24)-(26) become:

$$\alpha \frac{\partial \bar{c}}{\partial \bar{t}} = \frac{1}{\phi^2} \bar{\nabla}^2 \bar{c} - \bar{c}\bar{w} \tag{28}$$

$$\frac{\partial \bar{w}}{\partial \bar{t}} = -\bar{w} \int_0^1 \bar{c} d\bar{x} \tag{29}$$

$$\bar{c}|_{\bar{t}=0} = 0; \quad \bar{c}_{\bar{x}}|_{\bar{x}=0} = 0; \quad \bar{c}|_{\bar{x}=1} = 1; \quad \bar{w}|_{\bar{t}=0} = 1. \tag{30}$$

where

$$\alpha \equiv \frac{c^*}{w_0} \tag{31}$$

and

$$\phi \equiv \sqrt{\frac{k_2 w_0 L^2}{\mathcal{D}_l}} \tag{32}$$

is the *Theile Modulus*, which represents the relative significance of diffusion and reaction resistance.

We choose the following dimensionless variables for the SIP material:

$$c = c^* \bar{c}; \quad w = w_0 \bar{w}; \quad t = (k_2 c^*)^{-1} \bar{t}; \quad x = L_{\text{SIP}} \bar{x}. \tag{33}$$

The only difference is the change in the length scaling; we intentionally keep the time scaling consistent with the pure liquid case, in order to simplify the comparison of the absorption rates of the systems. With these dimensionless variables, equations (20), (22) and (23) become:

$$\alpha\beta \frac{\partial \bar{c}}{\partial \bar{t}} = \frac{1}{\bar{\phi}^2} \bar{\nabla}^2 \bar{c} - \xi \bar{c} \bar{w} \tag{34}$$

$$\frac{\partial \bar{w}}{\partial \bar{t}} = -\xi \bar{c} \bar{w}. \tag{35}$$

$$\bar{c}|_{\bar{t}=0} = 0; \quad \bar{c}_{\bar{x}}|_{\bar{x}=0} = 0; \quad \bar{c}|_{\bar{x}=1} = 1; \quad \bar{w}|_{\bar{t}=0} = 1. \tag{36}$$

where α is as above,

$$\beta = \frac{k_2}{k_2^{\text{eff}}} \tag{37}$$

and

$$\bar{\phi} = \sqrt{\frac{k_2^{\text{eff}} w_0 L_{\text{SIP}}^2}{\mathcal{D}^{\text{eff}}}} \tag{38}$$

is again the Thiele modulus of the material. The effectiveness factor is not a constant, as w may vary in space and time. Instead, it is given by:

$$\xi = \frac{\phi' \coth \phi' - 1}{\phi'^2/3} \tag{39}$$

where

$$\phi' = r_{\text{droplet}} \sqrt{\frac{k_2 w}{\mathcal{D}_l}} = \left(\frac{r_{\text{droplet}}}{L}\right) \phi \sqrt{\bar{w}} \tag{40}$$

where $\frac{r_{\text{droplet}}}{L}$ is a new dimensionless parameter, which quantifies the degree of separation between the microscopic and macroscopic scales. Overall, the dimensionless parameters describing absorption into the liquid are α and ϕ, and the parameters describing absorption into the SIP are α, β, ϕ, $\bar{\phi}$ and r_{droplet}/L.

4.4 Comparison of Saturation Times

We are interested in the ratio of the times, t_γ, required for each system to reach some arbitrary degree of saturation, γ:

$$\Psi \equiv \frac{t_\gamma^{\text{liq}}}{t_\gamma^{\text{SIP}}}. \tag{41}$$

This ratio will determine which material absorbs gas fastest: it may also be thought of as the ratio of the mean gas fluxes over the course of the gas absorption process. Because we have chosen the same dimensionless time scaling for each of our systems:

$$\Psi = \frac{\bar{t}_\gamma^{\text{liq}}}{\bar{t}_\gamma^{\text{SIP}}}. \tag{42}$$

Now, as can be seen from the non-dimensionalised equations, each of these $\bar{t}_\gamma$ values depends upon several dimensionless parameters:

$$\Psi = \frac{\bar{t}_\gamma^{\text{liq}}(\gamma, \alpha, \phi)}{\bar{t}_\gamma^{\text{SIP}}(\gamma, \alpha, \beta, \phi, \bar{\phi}, r_{\text{droplet}}/L)} \tag{43}$$

We can eliminate γ immediately by simply stipulating a reasonable value, such as 80% satuation ($\gamma = 0.8$). This still leaves α, β, the two Thiele moduli and r_{droplet}/L. The Thiele moduli may be related by:

$$\bar{\phi}^2 = \frac{k_2^{\text{eff}} w_0 L_{\text{SIP}}^2}{\mathcal{D}^{\text{eff}}} = \left(\frac{k_2 w_0 L^2}{\mathcal{D}_l}\right)\left(\frac{1-\varepsilon}{\varepsilon\frac{\mathcal{P}_s}{\mathcal{P}_l} + (1-\varepsilon)}\right)\left((1-\varepsilon) + \varepsilon\frac{\alpha}{\alpha+1}\frac{\mathcal{S}_s}{\mathcal{S}_l}\right)^{-2} \tag{44}$$

However, for this practical chemical system, $\alpha \ll 1$, and so

$$\bar{\phi}^2 \approx \phi^2 \left(\frac{1}{\varepsilon\frac{\mathcal{P}_s}{\mathcal{P}_l} + (1-\varepsilon)}\right)\frac{1}{(1-\varepsilon)} \tag{45}$$

or, more abstractly,

$$\bar{\phi} \approx \bar{\phi}\,(\varepsilon, \phi, \mathcal{P}_s/\mathcal{P}_l) \tag{46}$$

Overall then,

$$\Psi = \Psi(\alpha, \beta, \varepsilon, \phi, \mathcal{P}_s/\mathcal{P}_l, r_{\text{droplet}}/L). \tag{47}$$

However, consider the role of α and β in equations (34) and (28). In each case they are multipliers of the $\partial c/\partial t$ term. However, for systems with first-order reaction with diffusion, the concentration profile quickly asymptotes towards a stable quasi-steady state where $\partial c/\partial t \approx 0$, so that $\bar{\phi}^{-2}\bar{\nabla}^2\bar{c} \approx \bar{c}\bar{w}$. Given that $\alpha \ll 1$ and $\beta = \mathcal{O}(1)$, this asymptotic adjustment will happen extremely quickly (much faster than any changes in w) and the only effect of changing α or β will be to slightly increase or decrease the already very small time in which the concentration profile, c, takes to respond to changes in w. This will have negligible influence on the evolution of the concentration profiles and the gas uptake rate over time.

Numerical experiments confirmed this physical reasoning: starting from $\alpha = 10^{-2}$, $\beta = 1$, changing the value of either α or β by an order of magnitude only changed $\Psi_{0.8}$ by $\pm 1\%$.

Given this, it is clear that for a wide range of systems of practical interest:

$$\Psi = \Psi(\varepsilon, \phi, \mathcal{P}_s/\mathcal{P}_l, r_{\text{droplet}}/L). \tag{48}$$

The relationship between Ψ and ε is not particularly interesting (ε is constrained for practical reasons) and so we hold $\varepsilon = 0.5$. In this case,

$$\Psi = \Psi(\phi, \mathcal{P}_s/\mathcal{P}_l, r_{\text{droplet}}/L). \tag{49}$$

Numerical experiments sugest that Ψ is not sensitive to changes r_{droplet}/L for the large majority of SIPs. In particular, provided the internal droplets inside the SIP are ~ 20 times smaller than the macroscopic thickness of the SIP itself, then variations in Ψ do not significantly change

the absorption rate. This is unsurprising, as mass transfer in SIPs is typically controlled by *macroscopic* diffusion through the saturated zone shown in Fig 5a in the paper, rather than by *microscopic* diffusion inside the reaction zone. Hence Ho et al.[2], when modelling a similar system, ignored local reaction and diffusional resistances all together; the more complex model developed here collapses to their simpler model for a wide range of SIPs.

Hence, under most circumstances, $\Psi = \Psi(\phi, \mathcal{P}_s/\mathcal{P}_l)$. This is a very interesting result. It suggests that the improvement a SIP could provide over a static liquid depends upon only two factors: the relative permeability of the solid compared to the liquid (presumably the larger this is, the better for the SIP) and the Thiele modulus (which will capture the significance of the presence of the dead-zone, and also the case of $\phi \ll 1$, where reducing diffusional resistance is meaningless.)

The dimensionless equations for the SIP derived above were solved using the same discretisation scheme previously described, with the coefficients in the PDE and the initial conditions replaced by the relevant dimensionless numbers. The discretisation of the dimensionless equation for the static liquid was similar, except the $\dot{w}_i$ terms were replaced by the single term:

$$\dot{w} = -\frac{w}{m}\left(\frac{1}{2}(c_1 + c_{m+1}) + \sum_{i=2}^{m} c_i\right). \tag{50}$$

4.5 General Nondimensionalisation of Transport Equations.

For more complicated chemistries, the relationship between $\partial w/\partial t$ and c, w and the initial conditions may be much more complicated. In such cases, a dimensionless analysis can be simplified by considering the gas *loading*, λ, rather than the active species concentration. The gas loading is simply the amount of gas absorbed in the liquid, divided by the total chemical capacity of the gas. For chemical solvents, the physical solubility of the gas is typically ignored when calculating the loading. For a second order reaction, no matter how complicated the chemistry, the change in loading can always be expressed as:

$$\frac{\partial \lambda}{\partial t} = \frac{k_2 \xi c w}{N} \tag{51}$$

where N is the total amount of gas that can be chemically absorbed into the material per unit volume. If the reactive species concentration, w, is expressed in terms of the loading, then the differential equations for the SIP become:

$$\frac{\partial c}{\partial t} = \mathcal{D}^{\text{eff}} \nabla^2 c - k_2^{\text{eff}} \xi w(\lambda) c \tag{52}$$

$$\frac{\partial \lambda}{\partial t} = \frac{k_2 \xi c w(\lambda)}{N}. \tag{53}$$

with initial conditions,

$$c|_{t=0} = 0; \quad \lambda|_{t=0} = \lambda_0; \quad c_x|_{x=0} = 0; \quad c|_{x=L_{\text{SIP}}} = c^*. \tag{54}$$

For the liquid,

$$\frac{\partial c}{\partial t} = \mathcal{D}_l \frac{\partial^2 c}{\partial x^2} - k_2 c w(\lambda). \tag{55}$$

$$\frac{d\lambda}{dt} = \frac{k_2 w(\lambda)}{N} \frac{1}{L} \int_0^L c(x) dx. \tag{56}$$

The boundary and initial conditions are

$$c|_{t=0} = 0; \quad c_x|_{x=0} = 0; \quad c|_{x=L} = c^*; \quad \lambda|_{t=0} = \lambda_0. \tag{57}$$

For the SIP, the following dimensionless variables are defined:

$$t = \left(\frac{k_2 c^* w_0}{N}\right)^{-1} \bar{t}; \quad c = c^* \bar{c}; \quad x = L_{\text{SIP}} \bar{x} \tag{58}$$

where w_0 is a 'typical' reactive species concentration, which will be defined below. Then the differential equations become:

$$\alpha\beta \frac{\partial \bar{c}}{\partial \bar{t}} = \frac{1}{\bar{\phi}^2} \frac{\partial^2 \bar{c}}{\partial \bar{x}^2} - \xi \bar{c} \bar{w}(\lambda) \tag{59}$$

$$\frac{\partial \lambda}{\partial \bar{t}} = \xi \bar{c} \bar{w}(\lambda) \tag{60}$$

$$\bar{c}|_{\bar{t}=0} = 0; \quad \bar{c}_{\bar{x}}|_{\bar{x}=0} = 0; \quad \bar{c}|_{\bar{x}=1} = 1; \quad \lambda|_{\bar{t}=0} = \lambda_0. \tag{61}$$

where $\bar{w} \equiv w/w_0$, $\alpha \equiv c^*/N$, and otherwise all other variables are the same as above:

$$\beta = \frac{k_2}{k_2^{\text{eff}}} \tag{62}$$

and

$$\bar{\phi} = \sqrt{\frac{k_2^{\text{eff}} w_0 L_{\text{SIP}}^2}{\mathcal{D}^{\text{eff}}}} \tag{63}$$

For the liquid, the dimensionless variables are

$$t = \left(\frac{k_2 c^* w_0}{N}\right)^{-1} \bar{t}; \quad c = c^* \bar{c}; \quad x = L \bar{x} \tag{64}$$

giving the following dimensionless equations,

$$\alpha \frac{\partial \bar{c}}{\partial \bar{t}} = \frac{1}{\phi^2} \frac{\partial^2 \bar{c}}{\partial \bar{x}^2} - \bar{c} \bar{w}(\lambda) \tag{65}$$

$$\frac{\partial \lambda}{\partial \bar{t}} = \bar{w}(\lambda) \int_0^1 \bar{c} d\bar{x} \tag{66}$$

$$\bar{c}|_{\bar{t}=0} = 0; \quad \bar{c}_{\bar{x}}|_{\bar{x}=0} = 0; \quad \bar{c}|_{\bar{x}=1} = 1; \quad \lambda|_{\bar{t}=0} = \lambda_0. \tag{67}$$

where everything is the same as in the SIP, and

$$\phi = \sqrt{\frac{k_2 w_0 L^2}{\mathcal{D}_l}} \tag{68}$$

As before, $\alpha = c^*/N$ can be expected to be much less than unity for most practical chemical solvents. This means the analysis above is completely applicable, and $\Psi_\gamma = \Psi_\gamma(\varepsilon, \mathcal{P}_s/\mathcal{P}_l, \phi, r_{\text{droplet}}/L)$. Apart from $\varepsilon, \mathcal{P}_s/\mathcal{P}_l$, ξ and ϕ, the relative flux into the liquid and into the SIP depends only upon what may be called the 'chemistry' of the solvent: the function $w(\lambda)$. Physically, this represents the relationship between the solvent loading, λ, and the reactive species concentration in the solvent, w. However, it turns out that Ψ is relatively independent of $w(\lambda)$ if the quanitity w_0 is chosen appropriately. To demonstrate this, we consider 8 hypothetical 'chemistries' (i.e. $w(\lambda)$ functions):

- Direct consumption of active species: $w(\lambda) = 1 - \lambda$
- K2CO3 Solutions: $w(\lambda) = K_{eq} \frac{1-\lambda}{2\lambda}$
- Buffer of form $w \leftrightarrow 2B$: $w(\lambda) = (1-\lambda)^2$

- $w(\lambda) = 1 - \lambda + \sin(\pi\lambda)$
- $w(\lambda) = 1 - \lambda + \sin(5\pi\lambda)$
- $w(\lambda) = 1 - \lambda^2$
- $w(\lambda) = 1 - \sqrt{\lambda}$
- $w(\lambda) = 1 - \lambda^{0.1}$

Normalised versions of these are plotted in Figure S6. Some of these correspond to physical chemistries, while others are hypothetical relationships, chosen to capture as wide a range of relationships between the solvent loading and the active species concentration as possible (though all were required to satisfy $w(\lambda = 1) = 0$.) For each of these chemistries, and for each value of ϕ and $\mathcal{P}_s/\mathcal{P}_l$ in the phase diagram, the equations (59)-(66) were solved numerically using the methods described above. A continuous callback was built into the DE solver in order to find the exact time at which $\xi = 0.8$, and Ψ was recorded for each run. As discussed above, the plot was insenstive to the specific choice of α and β, and values of 0.01 and 1 were used. λ_0 was set equal to 0.1, primarily to avoid divide-by-zero errors in some $w(\lambda)$ functions. w_0 was set to the mean value of $w(\lambda)$ on the interval $\lambda \in [0.1, 1.0]$

$$w_0 = \int_{0.1}^{1} w(\lambda) d\lambda \tag{69}$$

This choice was made so that the Theile modulus, $\phi = \sqrt{k_2 w_0 L^2/\mathcal{D}_l}$ would most accurately reflect the dynamics inside the reaction zone in the liquid. With this choice of w_0, the value of Ψ was found to be largely independent of the shape of $w(\lambda)$, and near-identical phase diagrams were created for the wide range of chemistries plotted in Fig ES6. Without this adjustment (e.g. setting $w_0 = w(\lambda_0)$) the different chemistries do not converge to the same phase diagram.

5 Absorption of Carbon Dioxide into Carbonate Solutions.

Absorption of CO_2 into K_2CO_3-$KHCO_3$ buffer solutions is governed by the following chemistry:[5]

$$CO_2 + OH^- \xrightarrow{k_2} HCO_3^- \tag{70}$$

$$CO_3^{2-} + H_2O \rightleftharpoons HCO_3^- + OH^- \tag{71}$$

The second buffer reaction is considered to be instantaneous, and so the overall reaction is:

$$CO_2 + CO_3^{2-} + H_2O \longrightarrow 2\,HCO_3^- \tag{72}$$

with reaction rate given by:

$$r = -k_2[CO_2][OH^-]. \tag{73}$$

This chemistry is slightly more complicated than that discussed above. Our first task is to derive the function $f(\cdot,\cdot)$, giving the rate of change of reactive species,

$$\frac{\partial[OH^-]}{\partial t} = f([CO_2], [OH^-]). \tag{74}$$

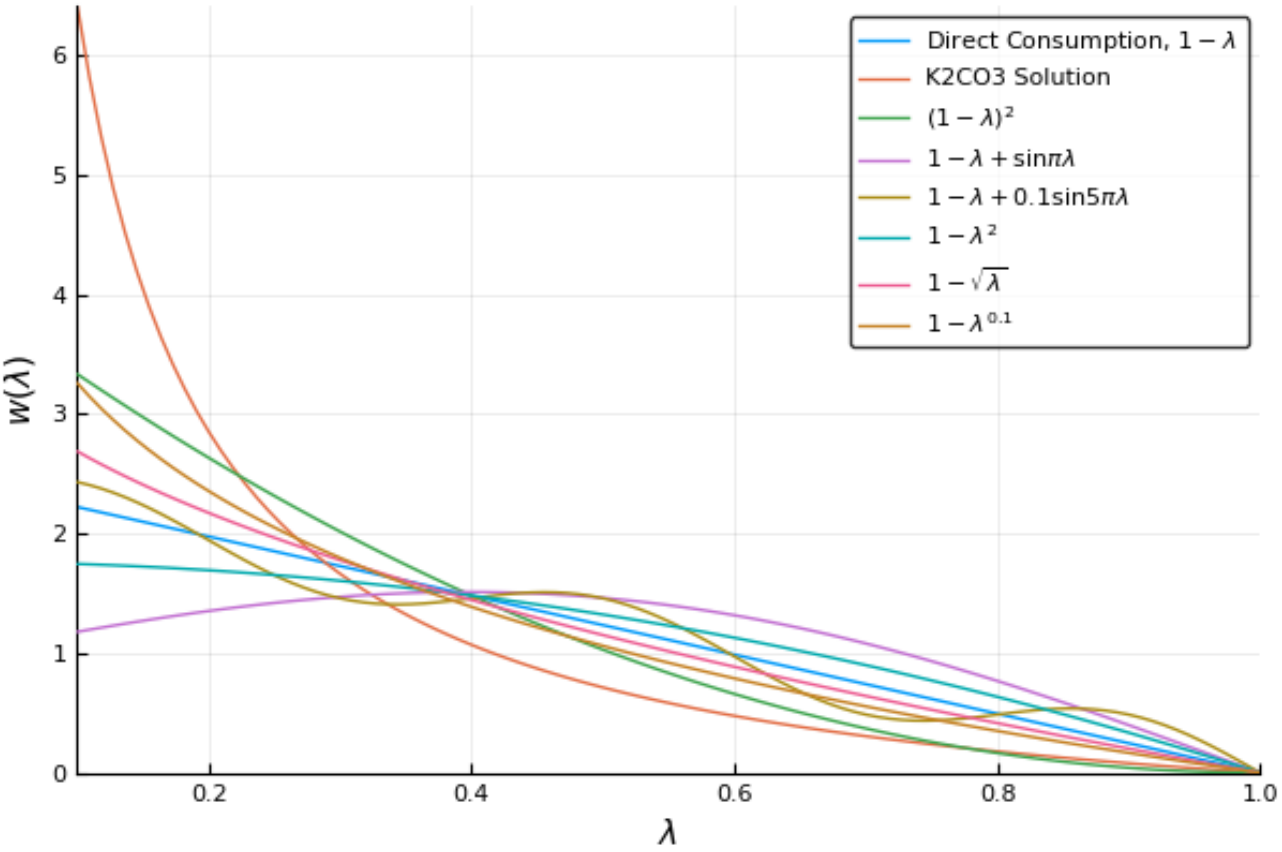

Figure S6: 8 chemistries used to create phase diagram in paper.

We first define the *loading* of carbon dioxide in the solvent:

$$\lambda \equiv \frac{0.5[\mathrm{HCO_3}^-]}{0.5[\mathrm{HCO_3}^-] + [\mathrm{CO_3}^{2-}]} = \frac{[\mathrm{HCO_3}^-]}{[\mathrm{HCO_3}^-] + 2[\mathrm{CO_3}^{2-}]} = \frac{[\mathrm{HCO_3}^-]}{2[\mathrm{CO_3}^{2-}]^0} \tag{75}$$

where $[\mathrm{CO_3}^{2-}]^0$ is the equivalent carbonate concentration (i.e. the concentration of carbonate if all $\mathrm{CO_2}$ were removed and all $\mathrm{HCO_3}^-$ were converted back to $\mathrm{CO_3}^{2-}$. For example, if a 3 M solution of $\mathrm{K_2CO_3}$ were created, then $[\mathrm{CO_3}^{2-}]^0$ would be 3 M, irrespective of the progression of (72).) The loading measures the overall progression of (72), and the rate of change of loading is given by:

$$\frac{\partial \lambda}{\partial t} = \frac{1}{2[\mathrm{CO_3}^{2-}]^0} \frac{\partial [\mathrm{HCO_3}^-]}{\partial t} = \frac{k_2[\mathrm{CO_2}][\mathrm{OH}^-]}{[\mathrm{CO_3}^{2-}]^0} \tag{76}$$

Furthermore, for the fast equilibrium reaction,

$$K_{eq} = \frac{[\mathrm{OH}^-][\mathrm{HCO_3}^-]}{[\mathrm{CO_3}^{2-}]}. \tag{77}$$

This may be written

$$\frac{[\mathrm{CO_3}^{2-}]}{[\mathrm{HCO_3}^-]} = \frac{[\mathrm{OH}^-]}{K_{eq}} \tag{78}$$

while (75) may be rearranged to give:

$$\frac{[\mathrm{CO_3}^{2-}]}{[\mathrm{HCO_3}^-]} = \frac{1-\lambda}{2\lambda} \tag{79}$$

and so overall

$$[\mathrm{OH}^-] = K_{eq} \frac{1-\lambda}{2\lambda} \tag{80}$$

This is the function $w(\lambda)$ considered in the dimensionall analysis above. If we rearrange (80), we get

$$\lambda = \frac{K_{eq}}{2[\mathrm{OH}^-] + K_{eq}}. \tag{81}$$

Taking the derivative of this last equation,

$$\frac{\partial \lambda}{\partial t} = \frac{\partial [\mathrm{OH}^-]}{\partial t} \left(\frac{-2K_{eq}}{(2[\mathrm{OH}^-] + K_{eq})^2} \right) \tag{82}$$

and comparing this with (76) gives:

$$f(c,w) = \frac{\partial [\mathrm{OH}^-]}{\partial t} = -\left(\frac{k_2 (2[\mathrm{OH}^-] + K_{eq})^2}{2K_{eq}[{\mathrm{CO}_3}^{2-}]^0} \right) [\mathrm{CO}_2][\mathrm{OH}^-] = -\left(\frac{k_2 (2w + K_{eq})^2}{2K_{eq}[{\mathrm{CO}_3}^{2-}]^0} \right) cw \tag{83}$$

This is our expression for $f(c,w)$, assuming that $\xi \approx 1$. If local diffusional resistance is significant, $f(\cdot)$ becomes

$$f(c,w,\xi) = -\xi \left(\frac{k_2 (2w + K_{eq})^2}{2K_{eq}[{\mathrm{CO}_3}^{2-}]^0} \right) cw \tag{84}$$

5.1 Properties of $\mathbf{K_2CO_3}$ Solutions.

5.1.1 Second-order Reaction Rate Constant k_{OH} in K2CO3 Solutions

Carbon dioxide reacts with hydroxide ions in the K_2CO_3 solution according to the following reaction:

$$\mathrm{CO}_2 + \mathrm{OH}^- \rightarrow {\mathrm{HCO}_3}^-$$

The second order rate constant for this reaction, k_{OH^-}, is, according to Astarita et al.[6], given by

$$k_{OH^-} = 10^{13.635 - 2895/T + 0.08I}$$

where T is the temperature in Kelvin, I the ionic strength in $\mathrm{mol\,L^{-1}}$, and k_{OH^-} has units of $\mathrm{L\,mol^{-1}\,s^{-1}}$.

5.1.2 Density of $\mathbf{K_2CO_3}$ Solutions

Novotny and Sohnel[7] provide functions for the density of salt solutions at various temperatures and concentrations:

$$\rho(t,c) = \rho_w(t) + (A + Bt + Ct^2)c + (D + Et + Ft^2)c^{3/2}$$

where t is the temperature in Celsius, c is the concentration in $\mathrm{mol\,L^{-1}}$, ρ_w is the density of pure water (in $\mathrm{kg\,m^{-3}}$, and $A, B, \ldots, F$ are constants. For the density of water, the function of Kell (1975) was used:

$$\rho(\mathrm{kg/m^3}) = \frac{999.83952 + 16.945176t - 7.9870401 \times 10^{-3} t^2 - 46.170461 \times 10^{-6} t^3}{1 + 16.897850 \times 10^{-3} t} + \frac{105.56302 \times 10^{-9} t^4 - 280.5423 \times 10^{-12} t^5}{1 + 16.897850 \times 10^{-3} t} \tag{85}$$

where t is again in degrees Celsius.

5.1.3 Viscosity of K_2CO_3 Solutions

The viscosity of potassium carbonate solutions was calculated using the correlation of Correia et al.:[8]

$$\mu(t,m) = \mu(t,0)\left(1 + \sum_{i=0}^{2}\sum_{j=0}^{2} f_{ij} t^i m^{j+1}\right)$$

Note that f_{ij} is a matrix of constants, t is temperature in degrees Celsius and their concentration unit, m, is molality, in mol/kg, see p. 203 of their paper. This calculation required a correlation for the viscosity of pure water as a function of temperature, and this is provided by Kestin, Sokolov and Wakeham:[9]

$$\log\left(\frac{\mu(t)}{\mu(20^oC)}\right) = \frac{20-t}{t+96}(1.2378 - 1.303\times10^{-3}(20-t) + 3.06\times10^{-6}(20-t)^2 + 2.55\times10^{-8}(20-t)^3)$$

where once again, t is the temperature in Celsius.

5.1.4 Diffusivity of CO_2 in K_2CO_3 Solutions

The diffusivity of carbon dioxide in potassium carbonate solutions is calculated from the diffusivity of CO_2 in pure water as measured by Versteeg and Van Swaalj:[10]

$$D_{CO2} = 2.35 \times 10^{-6} \exp(-2119/T)$$

where T is the temperature in Kelvin. This is modified for potassium carbonate solutions using the Stokes-Einstein relation, which simply states that $\mathcal{D} \propto 1/\mu$

5.1.5 Solubility of CO_2 in K_2CO_3 Solutions

We use the model of Weisenberger and Shumpe[11] to predict the solubility of CO_2 into dilute K_2CO_3 solutions. For more concentrated solutions, the parameters of Knuutila[12] are more appropriate.

The solubility, $\mathcal{S}_l$, in units $\mathrm{mol\,Pa^{-1}\,L^{-1}}$, are given by

$$\mathcal{S}_l = \mathcal{S}_{water} 10^{\sum(h_i + h_G)c_i}$$

where $\mathcal{S}_{water}$ is the solubility of the gas in pure water, h_i are the ion specific coefficients, c_i are the molar concentrations of the dissolved ions, and

$$h_G = h_{G,0} + (T - 298.15\mathrm{K})h_T$$

is the temperature-dependent parameter for the gas. For CO_2 dissolving in K_2CO_3, Weisenberger and Shumpe[11] give

- $h_{i,K} = 0.0922$ mol/L
- $h_{i,CO3} = 0.1423$ mol/L
- $h_{G0} = -0.172$ mol/L
- $h_T = -0.338 \times 10^{-3}$ mol/L.K

while Knuutila[12] gave parameters:

- $h_{i,K} = 0.0971$ L/mol

- $h_{i,CO3} = 0.1423$ L/mol
- $h_{G0,N2O} = -0.0085$ L/mol
- $h_{T,N2O} = -0.01809 \times 10^{-3}$ L/mol.K

Note that Knuutila's parameters are for N_2O, but they can be adjusted to CO_2 using the N_2O-analogy, which states that

$$\frac{S_{CO2} \text{ In Salt Soln.}}{S_{N2O} \text{ In Salt Soln.}} = \frac{S_{CO2}\text{In Water}}{S_{N2O} \text{ In Water}}$$

Finally, we need an expression for the solubility of CO_2 in water. The solubility, x_2, in units of mole fraction per atm, of CO_2 in water is given by Wilhelm et al.:[13]

$$R \ln x_2 = A + B/T + C \ln(T) + DT$$

where, for CO_2,

- $A = -317.658$ cal/K.mol
- $B = 17371.2$ cal/mol
- $C = 43.0607$ cal/K.mol
- $D = -0.00219107$ cal/K^2.mol
- $R = 1.987$ cal/K.mol

This gives almost identical results to the expression of Versteeg and Van Swaalj.[10]

5.1.6 Equilibrium Constant

The equilibrium constant

$$K_{eq} = \frac{[OH^-][HCO_3^-]}{[CO_3^{2-}]}$$

is given, at infinite dilution, by Hikita et al:[14]

$$K_{eq}^{\infty} = 10^{-1568.9/T + 2.5866 + 6.737 \times 10^{-3} T}$$

Where K_{eq}^{∞} has units $\mathrm{mol\,m^{-3}}$. It is common practice to describe VLE in these systems in terms of activity coefficient models such as the eNRTL model. However, the thermodynamic non-ideality can be corrected for by modifying the concentration-based equilibrium constant according to (Cents et al.[15]):

$$\log_{10} \frac{K_{eq}^{\infty}}{K_{eq}} = \frac{1.01\sqrt{c_{K^+}}}{1 + 1.49\sqrt{c_{K^+}}} + 6.1 \times 10^{-2} c_{K^+}$$

where c_{K^+} is the concentration of potassium ions in mol/L.

5.2 Absorption into a SIP Containing a Dilute K_2CO_3 Solution in a Closed Vessel

The model above must be slightly modified for mass transfer in a closed vessel, as which the partial pressure of the gas drops in proportion to how much gas has been absorbed:

$$p = p_0 - \frac{n_{abs} RT}{V_{vessel}} \tag{86}$$

Our model already tracks the total amount of gas absorbed, n_{abs}, and so this is a simple adjustment.

The function $f(c, w, \xi)$ was derived in (83), and is of the form:

$$f(c, w, \xi) = -\xi \left(\frac{k_2 (2w + K_{eq})^2}{2 K_{eq} c_{\mathrm{K_2CO_3}}} \right) wc \tag{87}$$

where k_2 is k_{OH}, K_{eq} is as defined in (77), and $c_{\mathrm{K_2CO_3}}$ is the concentration of the initial K_2CO_3 solution. An internal droplet size of $r_{\mathrm{drop}} = 15 \times 10^{-6}$ m was used to calculate ξ via Eq. (2), though, as noted above, the model is quite insensitive to the exact value of ξ.

The following volumes were measured for the fixed volume vessel and it's buffer tank. Each measurement was made 6 times, with an overall coefficient of variation of 0.35%.

- The Volume of the Reaction Vessel in which the SIP was placed was 0.3396 L. The volume of the SIP material was ignored.
- The Volume of the Buffer Tank from which CO_2 was supplied was 0.1803 L.

The values from the digital pressure gauge were also corrected using a recently callibrated gauge. The error was linear ($R^2 = 0.9998$) and so a simple linear correction was sufficient.

5.3 Justification of Statements from Paper.

We have the following statement from the 'Introduction' of the paper:

> For example, the permeability of CO_2 inside a 40wt% K_2CO_3 solution is about $8 \times 10^{-15}\,\mathrm{mol\,Pa^{-1}\,m^{-1}\,s^{-1}}$, while in the PDMS it is approximately $1 \times 10^{-12}\,\mathrm{mol\,Pa^{-1}\,m^{-1}\,s^{-1}}$, two orders of magnitude larger.

The value of $1 \times 10^{-12}\,\mathrm{mol\,Pa^{-1}\,m^{-1}\,s^{-1}}$ for the permeability of PDMS in CO_2 is widely cited - see the reference given in the paper. It is also consistent with our measured value for CO_2 into Semicosil in a 1 atm N_2 environment: we found a CO_2 diffusivity of $9.72 \times 10^{-10}\,\mathrm{m^2\,s^{-1}}$, and a solubility of $0.000\,78\,\mathrm{mol\,Pa^{-1}\,m^{-3}}$, giving a permeability of $7.6 \times 10^{-13}\,\mathrm{mol\,Pa^{-1}\,m^{-1}\,s^{-1}}$.

Before calculating the value of the permeability of CO_2 inside a 40wt% K_2CO_3 solution, we will also mention the following statement from the paper:

> For example, for a PDMS-based SIP containing 3wt% K_2CO_3, $\mathcal{P}_s/\mathcal{P}_l$ is only approximately 2, and so immobilisation is unlikely to increase the mean gas flux (see Supplementary Materials, section 5.3). On the other hand, for a PDMS-based SIP containing a 40wt% K_2CO_3 solution, $\mathcal{P}_s/\mathcal{P}_l \approx 120$, and solvent immobilisation could increase the gas flux by up to a factor of four, provided that $\phi \approx 10$, which corresponds to a thickness of ∼150 microns for this solvent (c.f. Fig 5e)

For both these statements, we must estimate the solubility of CO_2 in concentrated K_2CO_3 solutions. For such solutions, the parameters of Weisenberger and Shumpe[11] are inappropriate, and instead use the parameters of Knuutila et al.[12] We also calculate various values of $\frac{kw_0}{D}$ for Figure 5e using the correlations above. Finally, we use the values of $\frac{kw_0}{D}$ and the value $\phi \approx 10$ to calculate the thickness of the SIP, L_{SIP}. Using these correlations, we get the following values:

- The permeabilty of CO2 inside 3wt% K2CO3 is 5.14e-13 mol/Pa.m.s
- The permeabilty of CO2 inside 30wt% K2CO3 is 3.25e-14 mol/Pa.m.s
- The permeabilty of CO2 inside 40wt% K2CO3 is 7.89e-15 mol/Pa.m.s
- Taking the permeability of CO2 inside PDMS to be 1e-12 mol/Pa.m.s, Ps/Pl for 3wt% K2CO3 equals 1.94
- Taking the permeability of CO2 inside PDMS to be 1e-12 mol/Pa.m.s, Ps/Pl for 30wt% K2CO3 equals 30.68
- Taking the permeability of CO2 inside PDMS to be 1e-12 mol/Pa.m.s, Ps/Pl for 40wt% K2CO3 equals 126.64
- For 30 and 40wt% K2CO3 Solutions, the values of sqrt(D/kw0) are 1.696e-5 and 9.25e-6
- For 30 and 40wt% K2CO3 Solutions, the break-even thicknesses are 0.0006109, and 0.001479 m
- For 30 and 40wt% K2CO3 Solutions, the optimal thicknesses are 0.0001459, and 0.0001516 m

6 Bibliography for Supplementary Materials

1. Fogler, H. S. *Elements of chemical reaction engineering*; Prentice-Hall International London, 1999

2. Ho, W. S.; Hatton, T. A.; Lightfoot, E. N.; Li, N. N. Batch extraction with liquid surfactant membranes: a diffusion controlled model. *AIChE Journal*, **1982**, *28*, 662 – 670.

3. Hundsdorfer, W.; Verwer, J. G.; *Numerical Solution of Time-Dependent Advection-Diffusion-Reaction Equations*; Springer-Verlag, Berlin, 2010.

4. Hindmarsh, A. C.; Brown P. N.; Grant, K. E.; Lee, S. L.; Serban, R.; Shumaker, D. E.; Woodward, C. S. Sundials: Suite of Nonlinear and Differential/Algebraic Equation Solvers. *ACM Transactions on Mathematical Software* **2005**, *31*, 363–396.

5. Danckwerts, P. V. *Gas Liquid Reactions*; McGraw-Hill, 1970.

6. Astarita, G. *Gas Treating With Chemical Solvents*; Wiley, New York, 1983.

7. Sohnel, P.; Novotny, O. *Densities of Aqueous Solutions of Inorganic Substances*; Elsevier, 1985.

8. Correia, R.; Kestin, J.; Khalifa, H. Viscosity and density of aqueous sodium carbonate and potassium carbonate solutions in the temperature range 20 - 90 C and the pressure range 0 - 30 MPa. *Journal of Chemical and Engineering Data* **1980**, *25*, 201–206.

9. Kestin, J.; Sokolov, M.; Wakeham, W. Viscosity of liquid water in the range -8 C to 150C. *Journal of Physical and Chemical Reference Data* **1978**, *7*, 941 – 948.

10. Versteeg, G.; Van Swaalj, W. Solubility and diffusivity of acid gases (carbon dioxide, nitrous oxide) in aqueous alkanolamine solutions. *Journal of Chemical Engineering Data* **1988**, *33*, 29 – 34.

11. Weisenberger, S.; Schumpe, A. Estimation of gas solubilities in salt solutions at temperatures from 273 K to 363 K. *AIChE Journal* **1996**, *42*, 298 – 300.

12. Knuutila, H.; Juliussen, O.; Svendsen, H. Density and N2O solubility of sodium and potassium carbonate solutions in the temperature range 25 to 80 C. *Chemical Engineering Science*, **2010**, *65*, 2177 – 2182.

13. Wilhelm, E.; Battino, R.; Wilcock, R. Low-pressure solubility of gases in liquid water. *Chemical reviews* **1977**, *77*, 219 – 262.

14. Hikita, H.; Asai, S.; Takatsuka, T. Absorption of carbon dioxide into aqueous sodium hydroxide and sodium carbonate-bicarbonate solutions. *The Chemical Engineering Journal* **1976**, *11*, 131 – 141.

15. Cents, A.; Brilman, D.; Versteeg G. CO2 absorption in carbonate/bicarbonate solutions: The Danckwerts-criterion revisited. *Chemical Engineering Science* **2005** *60*, 5830 – 5835.